AD

AD-E404 259

Technical Report ARMET-TR-19036

THE DESIGN EVOLUTION OF SOFT DEPLOYABLE SHROUD FOR 120-MM IMAGE-BASED TERMINAL GUIDANCE MORTAR PROJECTILE

P. Stofko
R. Hanc
M. Mellini
C. Stout

December 2020

U.S. ARMY COMBAT CAPABILITIES DEVELOPMENT COMMAND ARMAMENTS CENTER

Munitions Engineering Technology Center

Picatinny Arsenal, New Jersey

The views, opinions, and/or findings contained in this report are those of the author(s) and should not be construed as an official Department of the Army position, policy, or decision, unless so designated by other documentation.

The citation in this report of the names of commercial firms or commercially available products or services does not constitute official endorsement by or approval of the U.S. Government.

Destroy by any means possible to prevent disclosure of contents or reconstruction of the document. Do not return to the originator.

REPORT DOCUMENTATION PAGE

Form Approved
OMB No. 0704-01-0188

1. REPORT DATE (DD-MM-YYYY)	2. REPORT TYPE	3. DATES COVERED (From - To)
December 2020	Final	10-01-2015 to 03-31-2018

4. TITLE AND SUBTITLE

The Design Evolution of Soft Deployable Shroud for 120-mm Image-based Terminal Guidance Mortar Projectile

5a. CONTRACT NUMBER

5b. GRANT NUMBER

5c. PROGRAM ELEMENT NUMBER

6. AUTHORS

P. Stofko, R. Hanc, M. Mellini, and C. Stout

5d. PROJECT NUMBER

5e. TASK NUMBER

5f. WORK UNIT NUMBER

7. PERFORMING ORGANIZATION NAME(S) AND ADDRESS(ES)

U.S. Army DEVCOM AC, METC
Armaments Engineering Analysis & Manufacturing Directorate (FCDD-ACM-AA)
Picatinny Arsenal, NJ 07806-5000

8. PERFORMING ORGANIZATION REPORT NUMBER

9. SPONSORING/MONITORING AGENCY NAME(S) AND ADDRESS(ES)

U.S. Army DEVCOM AC, ESIC
Knowledge & Process Management Office (FCDD-ACE-K)
Picatinny Arsenal, NJ 07806-5000

10. SPONSOR/MONITOR'S ACRONYM(S)

11. SPONSOR/MONITOR'S REPORT NUMBER(S)
Technical Report ARMET-TR-19036

12. DISTRIBUTION/AVAILABILITY STATEMENT

Approved for public release; distribution is unlimited.

13. SUPPLEMENTARY NOTES

14. ABSTRACT

The work presented here describes the design evolution of the thermally deployable shroud of an image-based, terminally-guided 120-mm mortar projectile. The design function, technical approach, finite element modeling, and testing were all described chronologically as the shroud was being developed. All preliminary testing suggests the design is successful. Additional actuation testing at various temperatures as well as live-fire testing is necessary to further prove out the function and survivability of the design at a relevant operating environment.

15. SUBJECT TERMS

Thermal-mechanical actuation Deployable shroud Discarding shroud Gun launch survivability

16. SECURITY CLASSIFICATION OF:			17. LIMITATION OF ABSTRACT	18. NUMBER OF PAGES	19a. NAME OF RESPONSIBLE PERSON
a. REPORT	b. ABSTRACT	c. THIS PAGE			P. Stofko
U	U	U	SAR	29	19b. TELEPHONE NUMBER (Include area code) (973) 724-1681

Standard Form 298 (Rev. 8/98)
Prescribed by ANSI Std. Z39.18

CONTENTS

FIGURES

FIGURES
(continued)

INTRODUCTION

The work presented here describes the development of the shroud for 120-mm mortar projectile's ogive with a nonpyrotechnic actuator for soft deployment to protect sensitive electronics. The Affordable Precision Technologies (APT), LLC, Virginia Beach, VA, project is the overarching Science & Technology initiative for next generation precision-guided munitions, which funded this shroud design and development activity. Described here is the design process and the role of finite element modeling to aid the design and development cycle. The shroud was specifically designed for enabling the technology of image-based terminal guidance (IBTG) for precision munitions in Global Positioning System (GPS) denied environments.

PURPOSE

As the name IBTG implies, the navigation is achieved by image tracking algorithms; therefore, imagers and lenses are incorporated in the projectile's ogive. In this specific case, day/night dual-imaging modes are achieved by having one visible and one long wave infrared (LWIR) imager side by side. In order to achieve the desired field of view, the physical size of the selected imagers and their lenses drives the requirement of 1.8-in. minimum diameter of the blunt face ogive. An aerodynamic analysis was conducted to determine the effect of said blunt nose on the range of flight of the projectile. Based on the results of this analysis, it was determined that the range of flight would be reduced by 5%. In order to maximize the range, it was required to design a shroud over the blunt ogive face depicted in figure 1 to provide a more aerodynamic shape to the nose of the round.

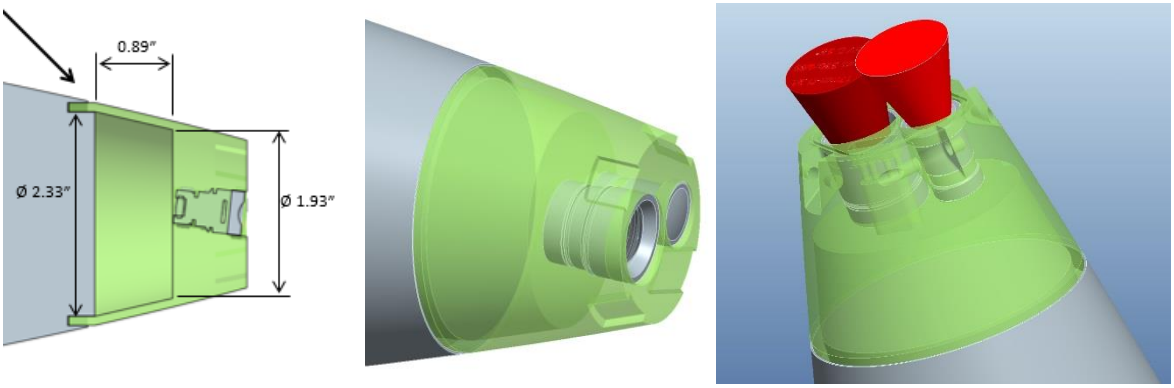

Figure 1
Blunt ogive

FUNCTIONAL DESIGN REQUIREMENTS

The main functions of the shroud are as follows: (1) to protect the lenses from physical damage and debris, (2) to provide aerodynamic drag reduction in order to maximize range, and (3) to act as a uniform defocused thermal surface for nonuniformity correction of LWIR imagers prior to operation. The shroud is mounted on the ogive of the projectile, butting up against the blunt face. During the first half of the trajectory, before apogee, the shroud is in the closed configuration. At a designated time in the flight path, the shroud discards from the projectile so that the imagers can begin gathering and processing image data for flight guidance. Imager data will be used mainly for terminal guidance, with the potential for horizon detection to obtain the preterminal orientation of the round. The shroud discard time is set to be prior to the deployment of canards to avoid possible

damage if the shroud petals were to collide with the canards. It is required for the shroud to be deployed with a “soft” mechanism because pyrotechnic discard mechanisms blackout inertial measurement units (IMU) for a short period of time, which affects guidance.

DESIGN CONCEPT

The initial concept for the shroud design is illustrated in figures 2, 3, and 4.

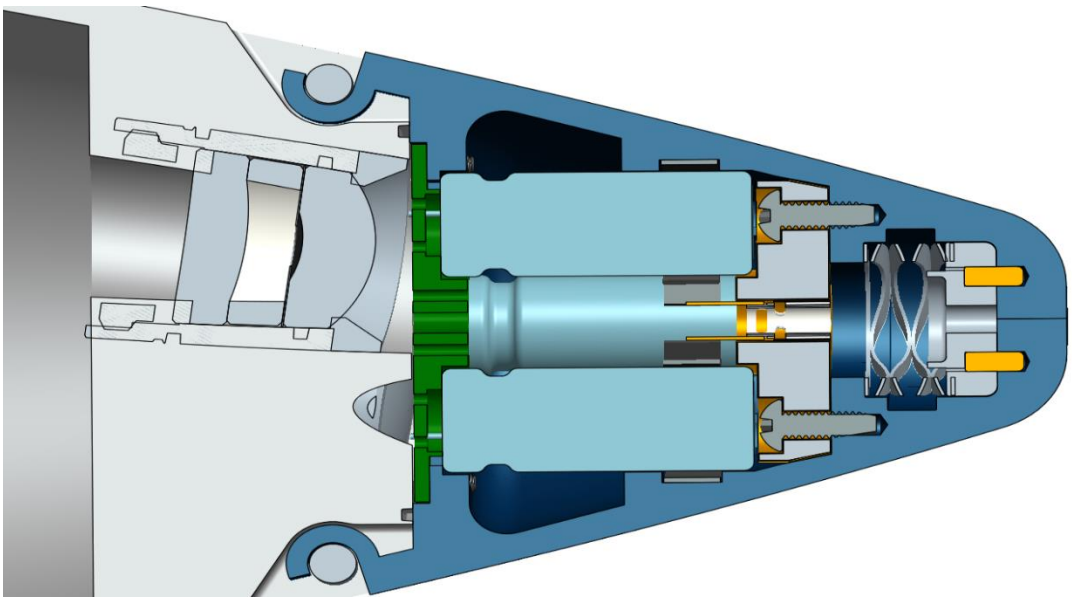

Figure 2
Shroud assembly cross section

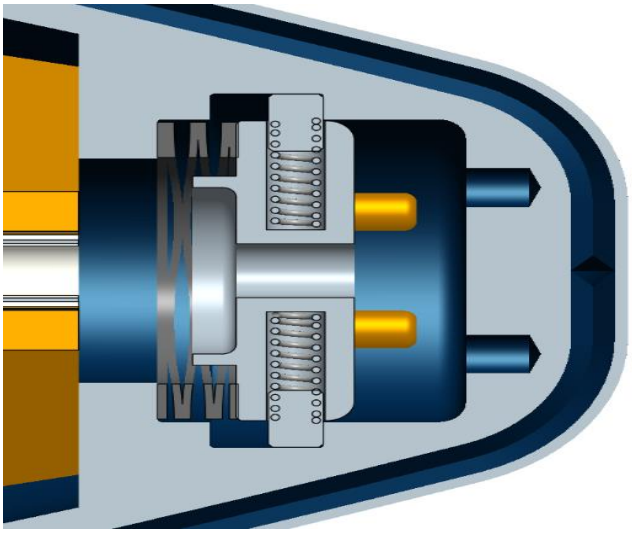

Figure 3
Bobbin mechanism

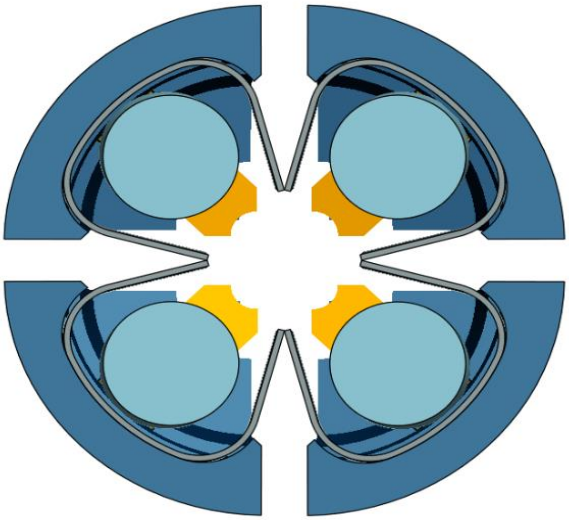

Figure 4
Leaf springs

The concept includes a safety bobbin mechanism, shown in figure 3, which is located in the front tip of the shroud. The mechanism keeps the shroud in a locked configuration during storage and transport. The bobbin mechanism disengages from the shroud petals after experiencing setback loading caused by the gun launch and is held in the unlocked state by side pins that extend radially outwards. From that point on, the only thing holding the shroud closed is a specially-designed solder joint in the middle of the shroud. This solder joint is made out of a low melting temperature alloy between a cylindrical ceramic heating element and four fingers spaced 90 deg apart (one for each petal). Upon command from the mission computer, the heating element melts the joint and releases the fingers, allowing the shroud to open. Each shroud petal subassembly contains a leaf spring that provides opening force against the adjacent petals, forcing them to open once the joint has melted. The heating element is powered by the capacitor bank that is located inside the shroud, one capacitor per petal. The shroud is also sealed to the environment via O-rings, which are installed in the petal grooves and on the ogive face of the projectile.

DETAILED DESIGN DESCRIPTION AND EVOLUTION

The Bobbin Mechanism

The safety bobbin consists of a simple spring mechanism. The wave spring pushes the bobbin forward keeping it engaged in the petal holes via dowel pins. The bobbin was designed to require 500 G's of acceleration to act for 0.002 sec in order to disengage it from the petals. There are two design variables determining this actuation. The first is the inertial force of the bobbin, which is dependent on its mass and is, therefore, a function of the material it is made out of. The second is the load generated by the compression spring. Due to the tight space claim, the wave spring was selected for its compact size at solid length (minimum compressed length of a spring). The bobbin material was selected to be aluminum so that the force generated by the mass of the bobbin at 500 G's acceleration would overcome the wave spring force and allow the bobbin to translate to the point where the spring-loaded side pins inside the bobbin can translate radially out into the radial groove around the bobbin. After the setback load stops acting on the bobbin, the wave spring, along with the setforward loading, act on the bobbin causing it translate forward. The extended side pins stop the bobbin from going too far and possibly re-engaging with the petal holes by physical contact of the pins hitting the end of the radial groove. Finite element simulation results in figure 5 show that

during this setforward action, the side pins will cause plastic deformation of 7% in a localized area of pin contact with the plastic petals. This amount of plastic deformation is acceptable because it is very local and the shroud only needs to function once.

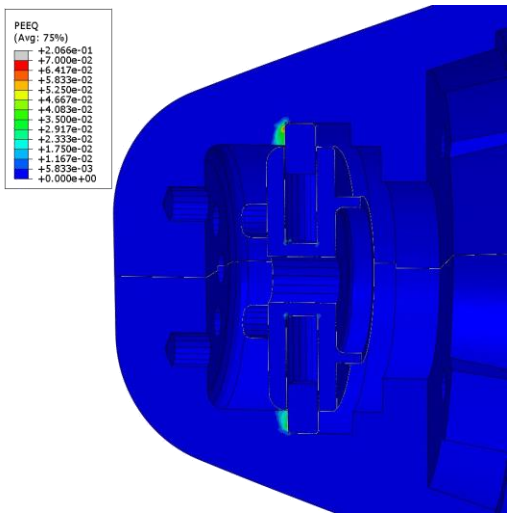

Figure 5
Equivalent plastic strain petal during bobbin pin impact

The petal material needs to be at least as strong as the modeled material, which was 30% glass-filled polycarbonate with a tensile yield strength of 16,000 psi. This also prevents the bobbin to be made out of any denser material than aluminum, which would only serve to increase this plastic deformation. If a larger acceleration force is required for bobbin disengagement, a flat metal washer could be inserted into the groove to provide a harder material surface at the pin contact interface. The wave spring plays a very minor role in the event, as most of the contact force is caused by the setforward acceleration. The wave spring only serves the purpose of keeping the bobbin initially engaged with the petal holes at the assembly level so that it does not disengage during standard transport induced vibrations and subsequent handling.

The Shroud Petal

The petals are designed as shown in figure 6, with features to provide support for the capacitors, leaf springs, heater fingers, and a circuit board for electrical connections to the projectile. The leaf springs are simply inserted into the grooves, the heater fingers are threaded into the petals, and the printed circuit boards (PCB) are also threaded but are additionally locked to the petal as well by the board cups.

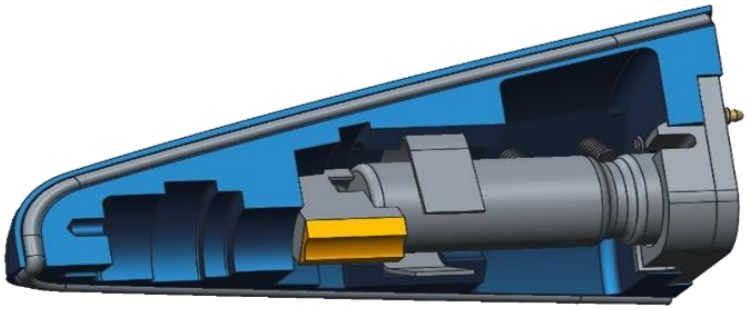

Figure 6
Petal subassembly

It was discovered by finite element simulation that the PCB being attached to the petal by only two 0 to 80-thread screws was not sufficient for gun launch survivability. The board cups were then additionally designed with snap features, as shown in figure 7, to provide extra locking support with the petal to minimize PCB deflection and increase survivability. They were made out of polycarbonate (Makrolon®) and manufactured by the injection molding process.

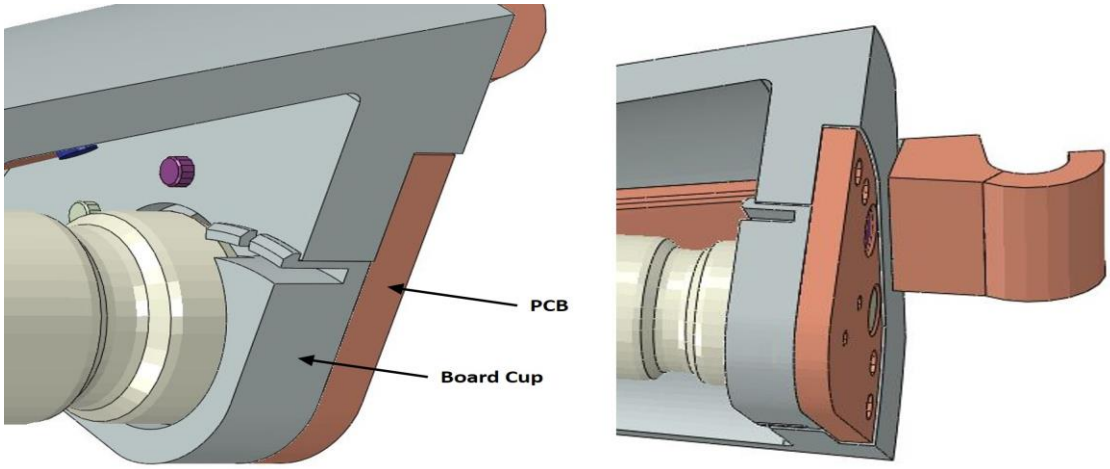

Figure 7
Additional support of PCB by board cup snap features

The petal also supports the aluminum hinge, which is inserted and locked into the petals with threaded fasteners. This method was selected for the prototype designs only, due to the ease of manufacturing this configuration. In the production design, the metal hinges would be overmolded during the manufacturing of the petals. The selected material for the petals is 30% glass-filled polycarbonate or polyetheretherketone (PEEK) to provide good impact resistance and higher tensile strength compared to an unfilled plastic. Initially, the petal and the hinge were designed as one single part made out of plastic, but finite element analysis (FEA) revealed that the plastic hinge would break from the setforward loading, and it was, therefore, redesigned as a separate part made out of aluminum. The petals are manufactured using the injection molding process, and all hole features and threads are post-machined. The O-ring grooves were designed with a V-shaped profile feature in the opening direction of the clamp mold in order to be created during the injection molding process. The petal hinge is shown in figure 8.

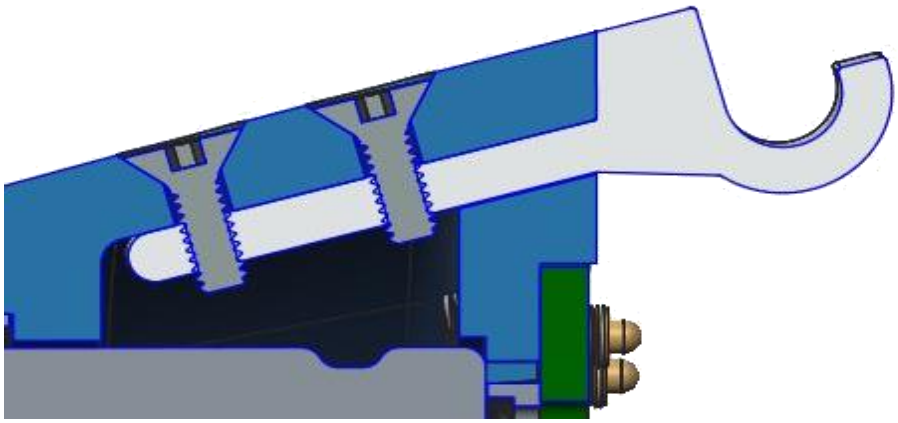

Figure 8
Petal hinge detail view

The Heater Finger

In order to attach the shroud petal to the heater element located along the center axis of the shroud, parts called heater fingers were designed to extend from the petal down to the outer diameter of the heater element. The heater fingers also contain a recessed feature to allow for clearance of the capacitors. The heater finger must have a metal surface in order to be soldered to the heater element and was designed to be machined completely out of metal; however, heat transfer FEA quickly uncovered a problem with heat conduction through this part. The heat was found to conduct very quickly up through the heater finger, taking heat away from the solder joint, which consequently could not heat up to the designed melting temperature.

This discovery led to the redesign of the heater finger, where only the material in close proximity to the solder area was to be constructed out of metal, while the rest of the component is plastic. Plastic materials have much lower ability to conduct heat compared to metal materials. The possible polymer options considered were polysulfone (PSU), polyimide (Kapton®), polyetherimide (Ultem™), and PEEK. These polymers were picked for their relatively high strength and maximum operating temperatures. The new design was necessary for maintaining the localized heat at the solder joint in order to melt the solder under 1 sec of time, but also it needed to be physically strong to survive the gun launch forces. Initial ideas to achieve this design consisted of an adhered, or electrolessly-plated, copper layer onto the plastic heater finger at the solder surface. The solder joint detail is shown in figure 9.

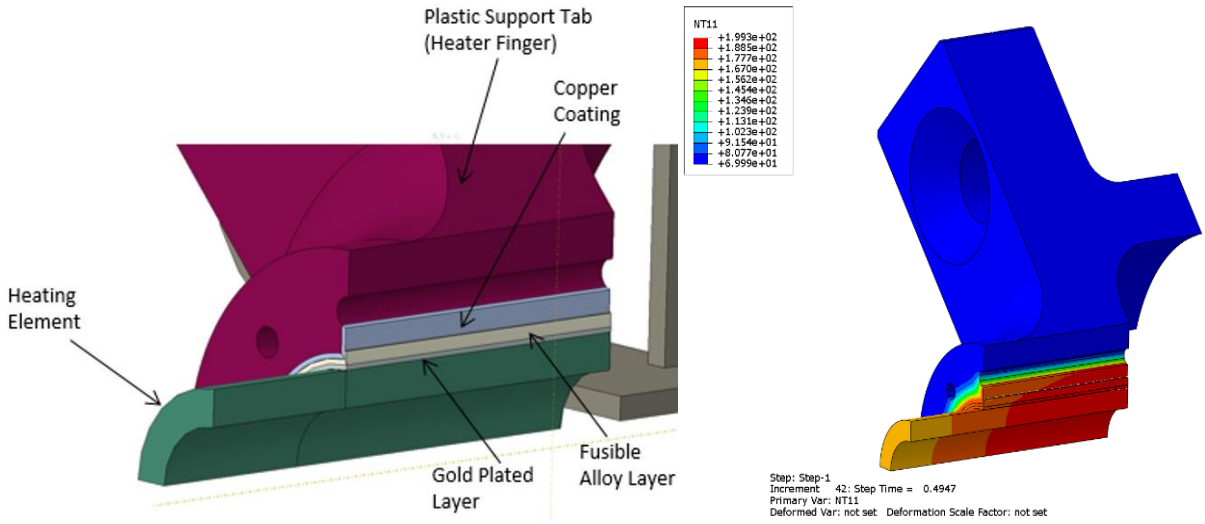

Figure 9
Solder joint detail view and heat transfer FEA

This design idea was investigated by testing different adhesives and electrolessly-plated samples for their shear strength. The shear strength values were then used to create material models for cohesive interfaces in FEA software. The joint concepts were simulated in the FEA code at gun launch loads as well as for thermal performance. This section will concentrate on the physical survivability, while the next section will cover the thermal performance results.

As for manufacturing of the prototype parts for this testing, the 0.003-in. thick copper foil was adhered to the cylindrical surface of the heater finger. Another version with electrolessly-plated copper layer is shown in figure 10.

Figure 10
Electrolessly-plated copper on plastic heater finger

Copper and PSU dog bones were machined and epoxied to each other initially using Hysol H3000 structural epoxy, also trying a cyanoacrylate type epoxy ZipGrip 2400TE later as an alternative option. Another set of copper-only samples were soldered together using the specific low melting temperature solder chosen for this application to compare the shear strength adhered versus soldered bonds. The samples were pulled in shear using an Instron machine under cold (-40 °F), ambient (70 °F), and hot (145 °F) environments. All dog bone mating surfaces were roughened with

a 600-grit sandpaper to generate 125-µ surface finish to help increase the strength of adhesion. Figure 11 shows the shear samples, and figure 12 shows the results of both the epoxy and solder shear tests.

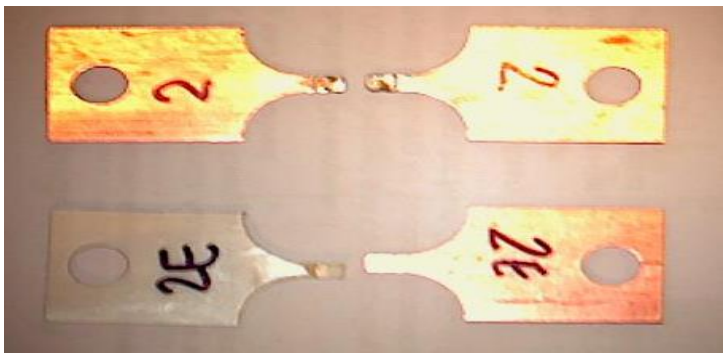

Figure 11
Shear samples

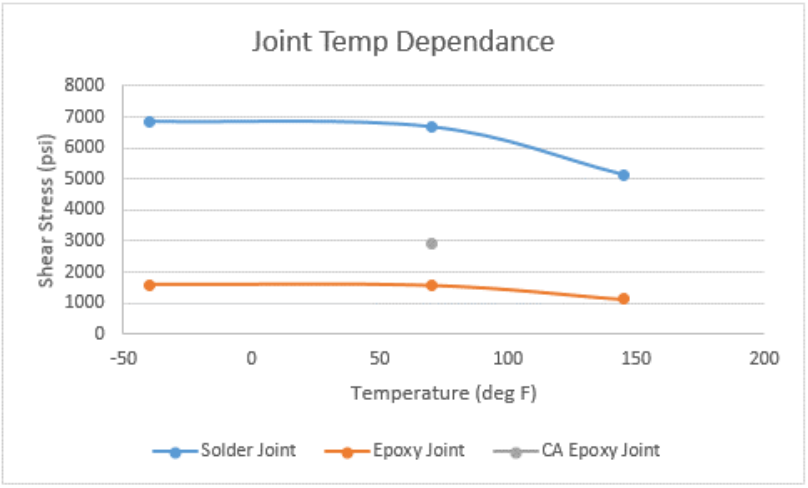

Figure 12
Shear strengths of solder and adhesive joints versus temperature

The concepts were also prototyped and tested using the air gun test facility at the U.S. Army Combat Capabilities Development Command (DEVCOM) Armaments Center (AC), Picatinny Arsenal, NJ. During testing, it was discovered that the solder joint was strong enough to withstand gun launch accelerations; however, the epoxy-adhered and electrolessly-plated surfaces were found to be too weak and failed at the interface between the copper foil/plating and plastic finger. The prototype hardware is shown in figure 13.

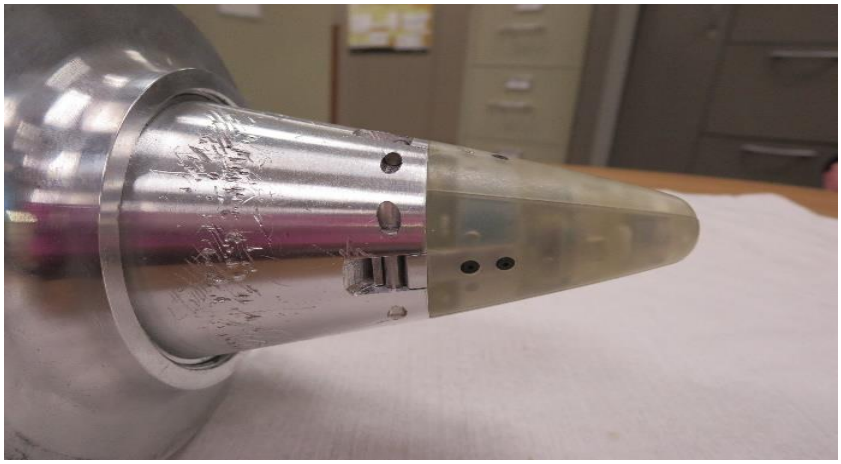

(a)
Hardware assembly before test

(b)
Premature shroud deployment due to adhesive joint failure after test

Figure 13
Prototype hardware

It was obvious that a stronger mechanical locking was needed for structural survivability at this interface. This realization led to the new threaded post design, where a threaded post would be machined on the opposite side of the thin cylindrical section of copper, which would then thread into the heater finger. The thread size and the cylindrical section thickness were carefully designed using structural and transient heat transfer FEA to provide the structural strength needed as well as meet the thermal performance necessary for the solder joint to absorb heat energy effectively. Results for structural FEA of this configuration can be seen in figure 14.

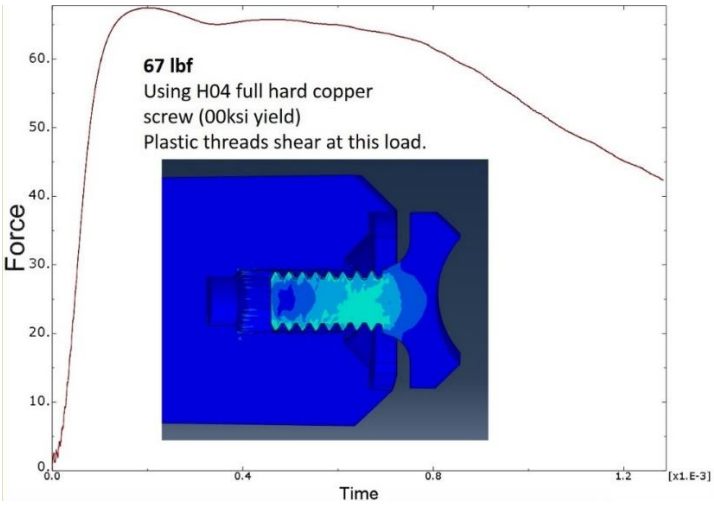

(a)
Structural FEA results- threaded post

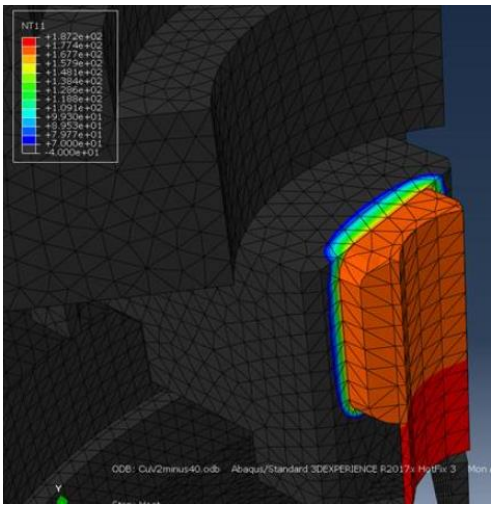

(b)
Thermal FEA results

Figure 14
Results for structural FEA of this configuration

This final threaded post design was again analyzed and tested using the gun launch accelerations and was found to survive with the shroud still in the closed configuration after the test. The safety bobbin was also observed to be disengaged and in the unlocked position as intended.

Heater Element and Power Source

The power requirement for the shroud was driven by the required heat transfer to achieve minimal time from sending an actuation signal to the actual shroud petal deployment. Due to the fact that this is a thermal actuation, the actuation time is, therefore, dependent on the ambient temperature. The extreme temperatures on either side of the operating temperature range (-45 to +145 °F) had to be considered to create the power requirement. Other factors, such as the surface area of the joint, the resistance of the heating element, the melting temperature of the fusible alloy,

the physical size of the capacitors, and the overall heat transfer from the heater to the adjacent shroud components, all played a significant role in determining the power requirements. The main design constraint in the super capacitor selection was its physical size due to the limited available space claim inside the shroud petals. Maximum physical size was selected for the available space claim in multiple configurations listed in table 1. The three studied configurations were based on the total energy the network can supply and its equivalent series resistance (ESR). Figure 15 shows the transient theoretical capacitor bank power discharge for each configuration.

Table 1
Capacitor bank configurations

HV0820-2R7305-R 0.08 ECR @ 100Hz (Ohms)

Option	Pairs			C (F)	V (V)	ESR (Ohm)	Energy (J)
X	X			X	X	X	X
X	X			X	X	X	X
1	4 in series			0.75	12	0.320	54.0
2	2 parallel networks of 2 in series			3	6	0.080	54.0
3	4 caps in parallel			12	3	0.020	54.0

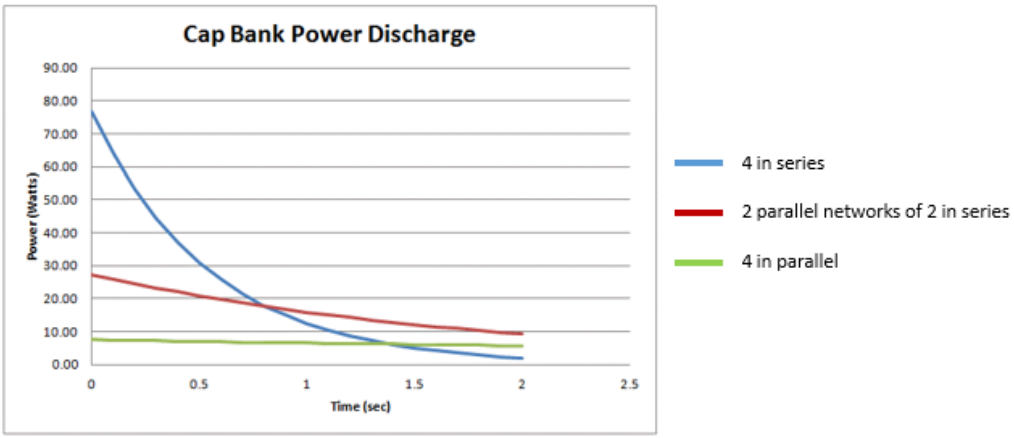

Figure 15
Capacitor power discharge

Table 2 shows the transient theoretical power discharge of configuration 2, having two parallel networks of two super capacitors in series. This configuration was selected based on the resistance of the heater and the maximum realistic current that could be handled by the leads going to the heater. The heater resistance and overall design were determined using heat transfer FEA. The power values from table 2 were generated by iteratively changing heater resistance values in the capacitor discharge equation:

$$I = \frac{V_0}{R} e^{-t/RC} \quad (1)$$

The R in the equation is the total R = R_{heater} + ESR_{cap}.

Table 2
Power input for transient heat transfer FEA

Time (sec)	Current (A)	Voltage (V)	Power (W)	Abaqus	Amp
0	4.88	6.00	27.36	171777.30	1
0.1	4.75	5.84	25.92	162714.70	0.947242
0.2	4.62	5.68	24.55	154130.21	0.897268
0.3	4.50	5.53	23.26	145998.63	0.84993
0.4	4.38	5.38	22.03	138296.05	0.805089
0.5	4.26	5.24	20.87	130999.85	0.762614
0.6	4.15	5.10	19.77	124088.57	0.722381
0.7	4.04	4.96	18.72	117541.93	0.684269
0.8	3.93	4.83	17.74	111340.66	0.648169
0.9	3.82	4.70	16.80	105466.57	0.613973
1	3.72	4.58	15.91	99902.37	0.581581
1.1	3.62	4.45	15.08	94631.74	0.550898
1.2	3.52	4.33	14.28	89639.17	0.521834
1.3	3.43	4.22	13.53	84910.00	0.494303
1.4	3.34	4.11	12.81	80430.33	0.468224
1.5	3.25	4.00	12.14	76186.99	0.443522
1.6	3.16	3.89	11.50	72167.53	0.420123
1.7	3.08	3.79	10.89	68360.12	0.397958
1.8	2.99	3.68	10.32	64753.59	0.376962
1.9	2.91	3.59	9.77	61337.33	0.357075
2	2.84	3.49	9.26	58101.30	0.338236

The derived power values served as the thermal energy input into the FEA analyses, which calculated the heat transfer from conduction among all the internal parts of the shroud. The obtained result was the time delay from the actuation trigger signal to the time the solder reached its full melting temperature. Analyses were performed at different ambient temperatures to cover the entire the operational temperature range of artillery projectiles.

The super capacitors were also tested at different temperatures to find the temperature dependency of the ESR. The results of the test are shown in figure 16. As expected, the colder the capacitors get, the more the ESR increases. Luckily, at the minimum operating temperature of -45 °F, the capacitor electrolyte is not yet frozen, and there is still good enough performance to achieve operation.

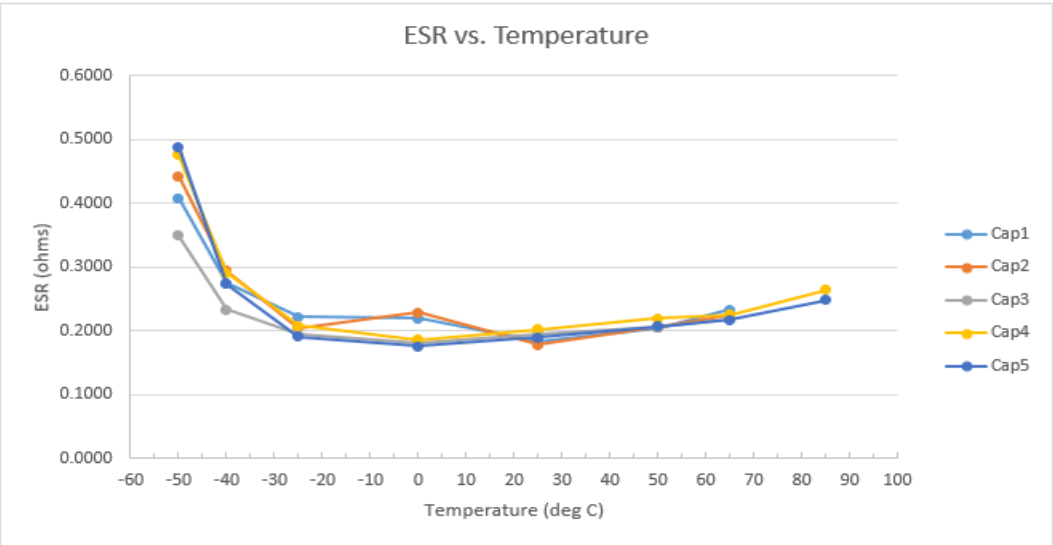

Figure 16
Super capacitor ESR versus temperature

In order to achieve the minimum actuation time, the surface area of the joint was limited in size considering the available power. However, it needed to be large enough to support the acceleration forces of the heating element in shear during setback and setforward of the gun launch event. All material selections were based on the heat transfer FEA simulation, iteratively solved until the minimum actuation time was achieved. The size and shape of the heater element was also driven by current manufacturing limitations. The very small size requirement coupled with high energy density requirement made it very difficult for industry experts to come up with a solution. Figure 17 shows the prototype of the heater element. The heater is made out of tungsten traces looped in layers to generate enough length to achieve the required resistance of ~1.2 ohms. These tungsten traces are printed on aluminum nitride (AlN) ceramic sheets, which are then rolled into a cylindrical shape and sintered. The AlN ceramic provides excellent thermal conductivity, dispersing the temperature field evenly and quickly through the heater's volume. In order to have a solder surface on the outside, the most outer layer of the AlN ceramic has a baked layer of tungsten coated over with nickel first and then coated over with gold.

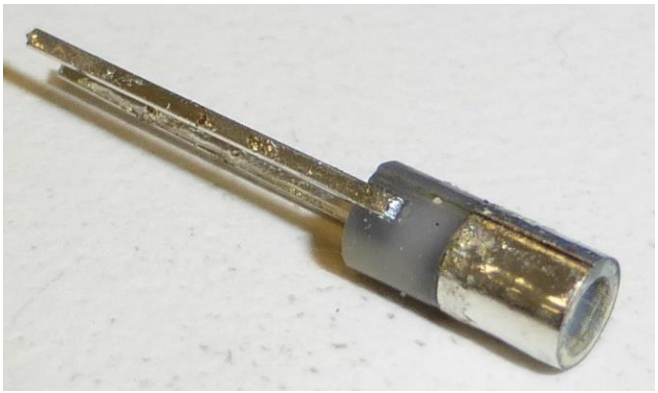

Figure 17
Prototype of heater element

The initial heaters were manufactured with a 16-µin layer of gold but were found to be too thin for proper tinning and resulted in a solder joint that was too weak. The heaters were sent back and replated to a total thickness of 50 µin of gold, which is a standard thickness on military grade connectors. This thickness of gold plating had no problem tinning the solder and maintaining a good solder joint.

Leaf Spring

As the solder melts and the fusible joint releases, the leaf springs provide radial force away from the center axis to generate a slight opening between the petals. The initial opening angle does not need to be large; it only needs to be sufficient enough for the air stream to enter the inside of the shroud and generate additional force to fully rotate the petals about the hinges and discard. In subsonic flight, pressure is generated along the ogive of the projectile such that it will force the shroud closed. Computational fluid dynamics (CFD) was ran to determine this dynamic pressure and determine the spring force necessary to open the shroud. The analysis was performed in STAR software, and the results are shown in figure 18.

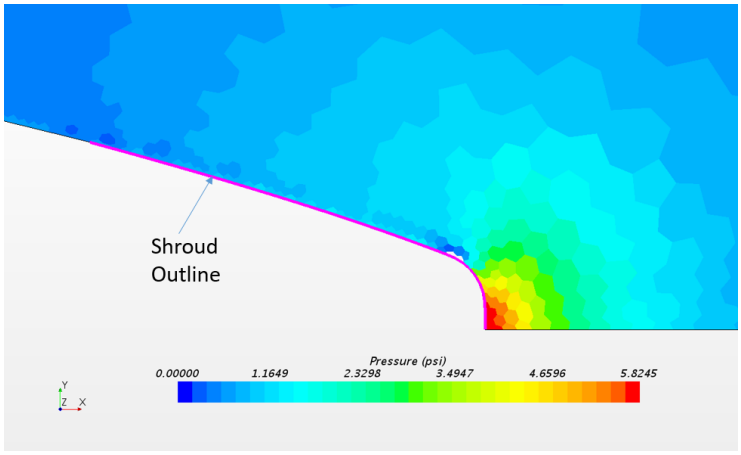

Figure 18
CFD results of dynamic pressure at 250-m/s velocity

Using the two-dimensional CFD results, the pressures along the outer surface of the shroud were extracted and summed to create an effective moment about the hinge. Since the hinge is out of the plane with most of the pressure forces, some of these pressure forces do not act about the hinge and ultimately cancel out due to the geometrical configuration of the shroud and hinge. The calculation for the minimum moment to open the hinge against 250-m/s air velocity is shown in figure 19 and the subsequent equation. The full derivation of the moment equation can be found in the appendix. Air speed of 250 m/s was analyzed to represent the expected muzzle velocity of this specific projectile during prototype testing.

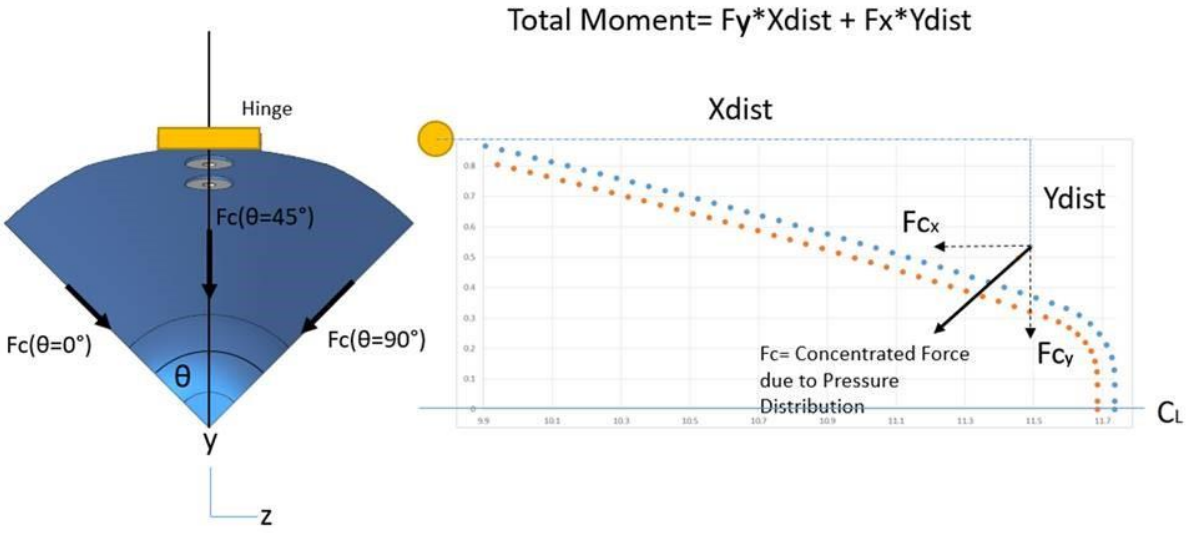

Figure 19
Pressure force Illustration on the shroud

$$M_{P_{dynamic}} = \left[Fc_{y0} \cdot X_{Hinge \rightarrow F_c} \cdot \left(2 \sin\left(\frac{\pi}{4}\right)\right)\right] + \left[Fc_x \cdot Y_{CL \rightarrow Hinge} \cdot \left(\frac{\pi}{2}\right)\right] - \left[Fc_x \cdot Y_{(CL \rightarrow F_c)_0} \cdot \left(2 \sin\left(\frac{\pi}{4}\right)\right)\right] \quad (2)$$

Include known values

F_{Cy_0}= 2.017 lbs
$X_{Hinge->F_c}$= 1.812 in
F_{Cx}= 1.988 lbs
$Y_{CL->Hinge}$ = .800 in
$Y_{(CL->F_c)_0}$ = .533 in

$$= \left[2.017 \cdot 1.812 \cdot (\sqrt{2})\right] + \left[1.988 \cdot .800 \cdot \left(\frac{\pi}{2}\right)\right] - \left[1.988 \cdot .533 \cdot (\sqrt{2})\right] = \boxed{6.17 \text{ in lbs}}$$

The final step of the leaf spring design was done using FEA to finalize the shape and thickness to achieve the necessary spring force within a reasonable stress level. American Iron and Steel Institute (AISI) 4340 steel was selected as a spring material to withstand the stresses and provide adequate force to overcome the hinge moment generated by the dynamic air pressure. Results of this structural analysis are shown in figure 20.

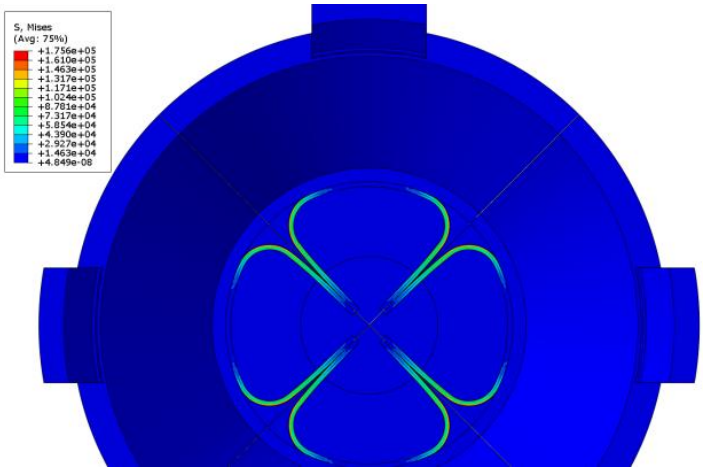

Figure 20
Leaf spring stress analysis at maximum load

The leaf spring performance was tested by mounting the fully assembled shroud into a wind tunnel at DEVCOM AC and externally triggering its deployment at three different Mach speeds: 0.2, 0.45, and 0.6. The shroud successfully deployed at all speeds. The shroud release during a wind tunnel test is displayed in figure 21.

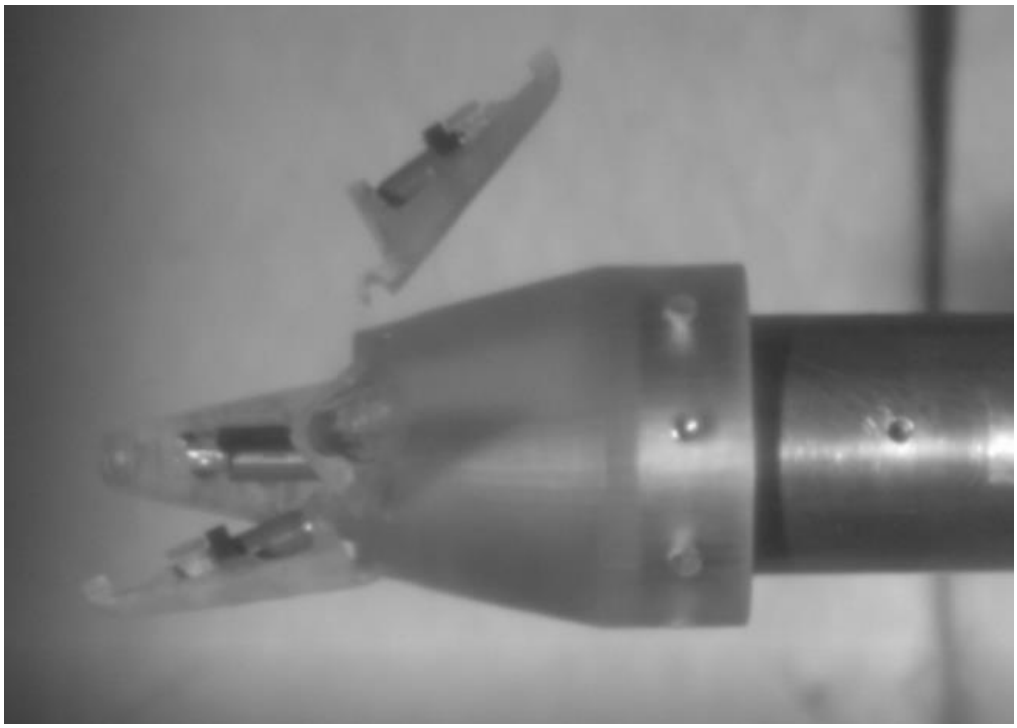

Figure 21
Wind tunnel test of shroud release

Electrical Connections

The shroud is electrically connected to the projectile by using spring plunger connections and custom receptacles shown in figure 22. The plungers are commercial off-the shelf components as well as the receptacles, but the receptacles were modified to have the front face chamfered to ensure better plunger contact, shortened, and redrilled due to the space claim constraints of the bulkhead. They were finally replated after these alterations with 50 μin of gold.

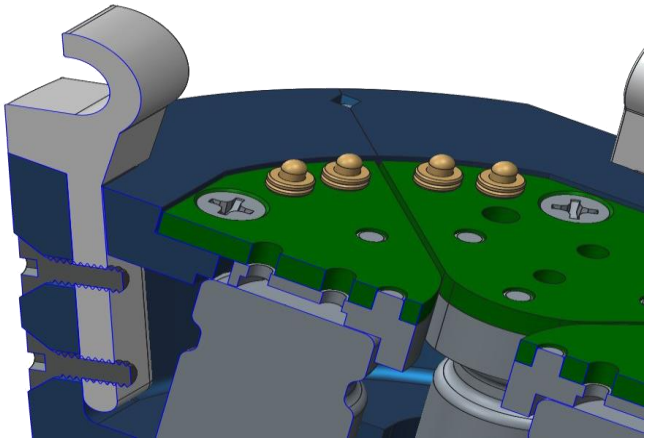

(a)
Plunger connectors

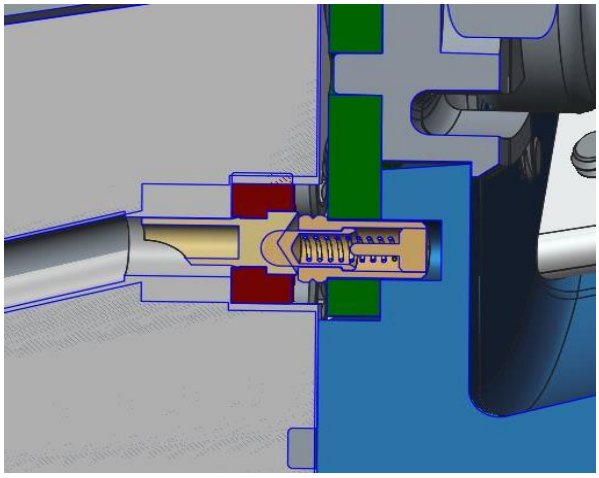

(b)
Connector cross section

Figure 22
Plunger connections and custom connectors

The spring plunger connectors, as well as the capacitor and heater leads, are soldered to the PCB boards. The heater ground is tied to the capacitor ground. The electrical schematic is shown figure 23.

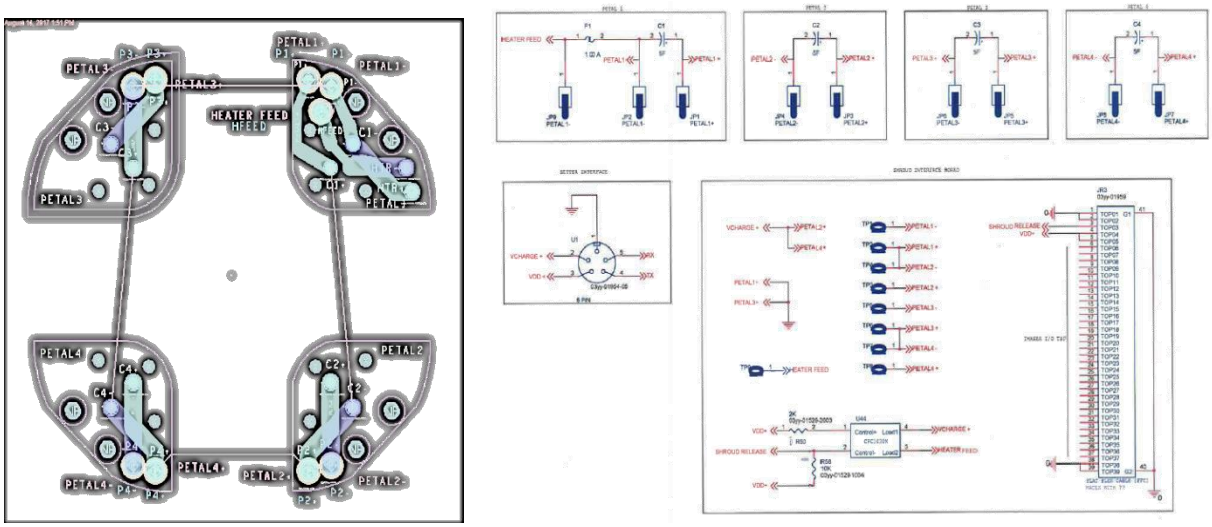

Figure 23
Shroud electrical schematic

CONCLUSIONS

The use of low melt temperature solder alloy as a fusible joint maintaining mechanical lock strong enough to survive the gun launch loads of 120-mm mortar was proven to be a feasible concept. The concept was successfully designed, prototypes were manufactured, and its functions were verified by testing in the laboratory environment. Also, the ability of designing and manufacturing a resistive heating element in such a small form factor, while achieving sufficient energy density for this actuation application, was also proven successful. This design has also proven to seal the imager lenses from gun gases while traveling inside the gun tube and to be a sufficient uniform optically defocused thermal surface for the nonuniformity correction of the infrared imager. Other similar armament related application for use of this concept is a canard or fin cover actuator mechanism. Additional performance testing is still required to be completed, including but not limited to: water sealing by submersion, sealing performance tests against blow-by gases, transport vibration testing, accelerated storage life testing at extremes temperatures, and functional performance testing at extreme ends of the operational temperature range. During the live-fire testing, an issue was discovered where the shroud could not properly deploy. This was believed to be caused by the spring plunger electrical connectors not allowing such high current to flow. The deployment functioned correcty when the heater was hardwired to the capacitor bank. Additional work will be needed to revise the electrical connections.

APPENDIX
DERIVATION OF MOMENT EQUATION

Pressure forces act normal to the surface on which they are applied, which in this case, generates forces that are out of plane with the rotation hinge of each nose cone petal. These pressures are weighted and summed over a 2-dimensional surface to be represented as a concentrated x and y force that will contribute to the generated moment about the hinge. Since the hinge is located on the center plane of the petal as shown below, the out of plane (z-component) forces will net to 0, and the remaining y-direction forces will have a weaker effect on the hinge moment due to their lesser magnitude.

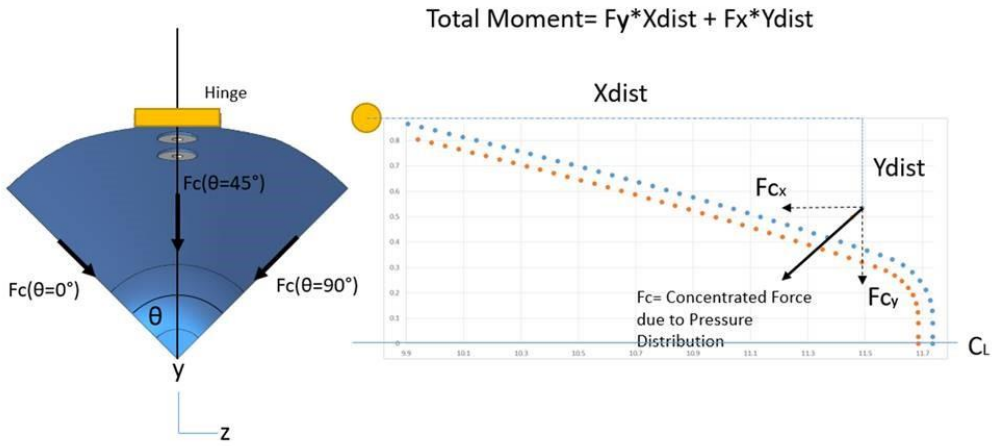

The forces in the y-direction (in plane with the hinge) then become a function of theta, as well as the y-distance at which the concentrated force acts.

$$HingeMoment = \int_0^{\frac{\pi}{2}} Fc_y(\theta) * Xdist\, d\theta + \int_0^{\frac{\pi}{2}} Fc_x * Y_{dist}(\theta)\, d\theta$$

$$Fc_y(\theta) = Fc_{y0} * \cos\left(\frac{\pi}{4} - \theta\right)$$

Where,
Fc_{y0}: Concentrated Y force at max conditions ((θ=45°)

Therefore $Fc_y(\theta = 45°) = Fc_{y0}$

$$Y_{dist}(\theta) = Y_{CL\to Hinge} - Y_{(CL\to F_c)_0} \cos\left(\frac{\pi}{4} - \theta\right)$$

Where,
$Y_{CL\to Hinge}$: Y distance from centerline to hinge
$Y_{(CL\to F_c)_0}$: Y distance from centerline to force concentration @ max conditions (θ=45°)

Therefore $Y_{dist}(\theta = 45°) = Y_{CL\to Hinge} - Y_{(CL\to F_c)_0}$

Substituting Functions of θ

$$HingeMoment = \int_0^{\frac{\pi}{2}} \left(Fc_{y0} \cdot \cos\left(\frac{\pi}{4} - \theta\right)\right) \cdot X_{Hinge\to F_c}\, d\theta + \int_0^{\frac{\pi}{2}} Fc_x \cdot \left(Y_{CL\to Hinge} - Y_{(CL\to F_c)_0} \cos\left(\frac{\pi}{4} - \theta\right)\right) d\theta$$

$$= \left[Fc_{y0} \cdot X_{Hinge\to F_c} \int_0^{\frac{\pi}{2}} \cos\left(\frac{\pi}{4} - \theta\right) d\theta\right] + \left[Fc_x \cdot Y_{CL\to Hinge} \int_0^{\frac{\pi}{2}} d\theta\right] - \left[Fc_x \cdot Y_{(CL\to F_c)_0} \int_0^{\frac{\pi}{2}} \cos\left(\frac{\pi}{4} - \theta\right) d\theta\right]$$

Integrate & evaluate at limits

$$= \left[Fc_{y0} \cdot X_{Hinge\to F_c} \cdot \left(-\sin\left(\frac{\pi}{4} - \frac{\pi}{2}\right) + \sin\left(\frac{\pi}{4}\right)\right)\right] + \left[Fc_x \cdot Y_{CL\to Hinge} \cdot \left(\frac{\pi}{2}\right)\right] - \left[Fc_x \cdot Y_{(CL\to F_c)_0} \cdot \left(-\sin\left(\frac{\pi}{4} - \frac{\pi}{2}\right) + \sin\left(\frac{\pi}{4}\right)\right)\right]$$

Simplify

$$M_{P_{dynamic}} = \left[Fc_{y0} \cdot X_{Hinge\to F_c} \cdot \left(2\sin\left(\frac{\pi}{4}\right)\right)\right] + \left[Fc_x \cdot Y_{CL\to Hinge} \cdot \left(\frac{\pi}{2}\right)\right] - \left[Fc_x \cdot Y_{(CL\to F_c)_0} \cdot \left(2\sin\left(\frac{\pi}{4}\right)\right)\right]$$

BIBLIOGRAPHY

1. Stofko, P., Mellini, M., and Stout, C., “Thermally Deployable Shroud for Affordable Precision Guided Projectile,” U.S. Patent no. 10030952 B1, U.S. Army, July 2018.

DISTRIBUTION LIST

U.S. Army DEVCOM AC
ATTN: FCDD-ACE-K
FCDD-ACM- AA, P. Stofko
R. Hanc
FCDD-ACM-FP, M. Mellini
C. Stout
Picatinny Arsenal, NJ 07806-5000

Defense Technical Information Center (DTIC)
ATTN: Accessions Division
8725 John J. Kingman Road, Ste. 0944
Fort Belvoir, VA 22060-6218

GIDEP Operations Center
P.O. Box 8000
Corona, CA 91718-8000
gidep@gidep.org

REVIEW AND APPROVAL OF ARDEC TECHNICAL REPORTS

THE DESIGN EVOLUTION OF SOFT DEPLOYABLE SHROUD FOR 120MM IMAGE BASED TERMINAL GUIDANCE MORTAR PROJECTILE
Title

Date received by LCSD

PAVOL STOFKO, R. HANC, M. MELLINI, C. STOUT
Author/Project Engineer

Report number (to be assigned by LCSD)

x1681 — Extension
B. 94 — Building

RDAR-MEA-A
Author's/Project Engineers Office (Division, Laboratory, Symbol)

PART 1. **Must be signed before the report can be edited.**

a. The draft copy of this report has been reviewed for technical accuracy and is approved for editing.

b. Use Distribution Statement A X, B____, C____, D____, E____, F____ or X____ for the reason checked on the continuation of this form. Reason: _____

1. If Statement A is selected, the report will be released to the National Technical Information Service (NTIS) for sale to the general public. Only unclassified reports whose distribution is not limited or controlled in any way are released to NTIS.

2. If Statement B, C, D, E, F, or X is selected, the report will be released to the Defense Technical Information Center (DTIC) which will limit distribution according to the conditions indicated in the statement.

c. The distribution list for this report has been reviewed for accuracy and completeness.

Edward Bauer 3/12/19
Division Chief (Date)

PART 2. To be signed either when draft report is submitted or after review of reproduction copy.

This report is approved for publication.

Edward Bauer
Division Chief (Date)

Arnold Klein 3/15/19
RDAR-CIS (Date)

LCSD 49 supersedes SMCAR Form 49, 20 Dec 06